SYNERGETIC EFFECTS DURING CO-PYROLYSIS OF WOODY BIOMASS AND ZHUNDONG COAL

Shuanghui Deng, Zhicheng Fu, Houzhang Tan*, Zhong Xia, Xuebin Wang, Renhui Ruan

MOE Key Laboratory of Thermo-Fluid Science and Engineering, Xi'an Jiaotong University, Xi'an, Shaanxi, 710049, China

*Corresponding author: Houzhang Tan (Email: hzt@xjtu.edu.cn)

Co-pyrolysis of biomass and coal is a promising way to produce liquid and char products while contributing to reduce CO_2 emission. The co-pyrolysis behaviors and characteristics of poplar sawdust (PS) with Zhundong coal (ZD) in the different blending ratios were investigated using a thermogravimetry analyzer (TGA) in this work. The results indicated that compared with ZD, PS had a lower characteristic temperature of volatile matter release and a stronger pyrolysis reactivity. There were synergistic promoting and inhibiting effects in the whole co-pyrolysis process of PS and ZD, which were related to the blending ratio. The PS addition percentage of 20, 40 and 80% into ZD presented the obvious positive synergistic interactions in the co-pyrolysis process, enhancing the thermal decomposition rate of volatile compounds. The important kinetic parameters were obtained using the first-order reaction model. Adding PS into ZD in the pyrolysis process changed the porous structure and surface morphology of ZD char particles. The results obtained are expected to be helpful in the equipment design and practical application of biomass and ZD co-pyrolysis.

Keywords: Biomass, Zhundong coal, Co-pyrolysis, Synergistic effect, Kinetic

1. Introduction

Biomass is being considered as a clean and sustainable energy because of its widespread sources, low pollutant emissions and near-zero CO_2 emission [1]. However, biomass has several defects, such as high moisture content, low heating value, lower bulk density and so on [2]. These shortcomings cause biomass hard to be applied in a large scale. The co-utilization of biomass and Zhundong coal (ZD) is an important way to overcome the disadvantage of using biomass alone and effectively use the advantage of biomass resources. ZD is a great wealth of natural resource in China with prognostic reserves of 390 billion tons, enough to meet current Chinese energy demand for many years [3]. ZD ranges from lignite to sub-bituminous, which is obvious characterized by low contents of ash and sulfur as well as moderate calorific value. However, the treatment and utilization of ZD produce a large amount of harmful substances and greenhouse gases, such as sulfur dioxide, nitrogen oxides

and CO_2, which are not only inefficient but also cause irreversible damage to the environment. Additionally, ZD has a high level of alkali/alkaline earth metal species (AAEMs) which cause ash-related problems in the furnace wall and heat exchange surface of boilers, such as slagging, fouling and sintering. Under the strict energy conservation and environmental protection policies, a primary concern with ZD utilization is effective reduce and low emission of harmful substances and CO_2 [4].

Gaseous pollutants derived from ZD combustion contribute a lot to health-threatening environmental issues. Therefore, co-utilization of biomass and ZD has become a popular technique recently, trying to break restrictions of thermochemical utilization technologies of coal. Biomass co-combustion in a coal-fired plant may be a more feasible way from the perspective of energy utilization and CO_2 reduce. This way has some economic advantages. For instance, there is no need to add new employees, and the existing facilities and devices of gases clean and emission control can be used. Consequently, no additional investments are needed in a new co-combustion processing plant. In sight of environment protection, biomass co-combustion with ZD can help reduce coal consumption and CO_2 emission. Pyrolysis is the first step in the thermochemical conversion processes including gasification and combustion, therefore it has a significant impact on subsequent reactions. The products from biomass pyrolysis show higher heating values than raw biomass [5]. Although there have been some reports on the co-pyrolysis characteristics of biomass and coal [6, 7], the study on biomass co-pyrolysis with ZD is still rare. The research on the co-pyrolysis process of biomass and ZD would help establish the foundations for ZD further studies on other thermochemical reactions and relevant industrial application. Combined biomass and ZD as feedstock for energy production can offer several advantages in terms of environmental improvement, economy promotion and biomass energy utilization. The biggest attractive technical edge of such a co-pyrolysis way is that synergistic effects or interaction possibly occurs between biomass and ZD.

Currently, a number of studies have showed that there are different synergetic effects in the co-processing of biomass and other types of coal, in particular co-pyrolysis [8-10]. Additionally, some researches have not considered the significant synergetic effects when using biomass and other types of coal blends. Although there are many studies on biomass co-pyrolysis in literature, few researches have elaborated on biomass co-pyrolysis with ZD. Moreover, the co-pyrolysis technology of biomass with ZD has an excellent industrial application prospect in China. Further study is still essential to explore the co-pyrolysis behaviors of biomass with ZD and their interactions due to the complicated compositions of biomass and the diversities of ZD. Therefore, this work investigated woody biomass co-pyrolysis behaviors with ZD. Subsequently, their co-pyrolysis characteristics and kinetic parameters were given. The fundamental knowledge and basic data obtained from this work are essential for the proper understanding and application of biomass co-pyrolysis/co-firing with ZD in the practical pulverized fuel based systems.

2. Samples and methods

2.1. Sample properties

In this work, poplar sawdust (PS) was chosen as woody biomass sample for its typical representativeness in China. A type of ZD was chosen as coal sample for its extensive application in power generation. Raw PS was collected from a wood processing factory in Xi'an, Shaanxi Province, China, and ZD was acquired from a ZD mine located in Xinjiang Province, China. PS and ZD were dried in an oven at 105 ^{o}C for 48 h to eliminate the effect of external moisture. According to the test analysis and the relevant study [11], the results on the proximate and ultimate analysis of PS and ZD are listed in Tab. 1, and the ash compositions are presented in Tab. 2. The dried PS and ZD were grounded and sieved to less than 200 μm. After that, PS and ZD were blended together, with PS mass percentages of 20, 40, 60 and 80%.

Tab. 1. Proximate and ultimate analysis of PS and ZD samples

Samples	Proximate analysis/wt%			Ultimate analysis/wt%				
	A_d	V_d	FC_d	C_d	H_d	N_d	O_d	$S_{t,d}$
PS	7.36	83.19	9.45	51.02	6.81	3.39	46.79	0.01
ZD	8.50	28.24	63.26	72.84	3.22	0.64	14.22	0.45

d represents the dry basis.

Tab. 2. Compositions of PS and ZD ash samples

Samples	Ash compositions/wt%								
	Fe_2O_3	K_2O	Na_2O	MgO	CaO	SO_3	Al_2O_3	SiO_2	Others
PS	0.00	6.86	19.00	21.30	13.85	2.43	10.90	22.53	3.13
ZD	8.02	0.55	6.07	6.60	40.69	11.32	7.68	17.38	1.69

According to the results in Tab. 1, the volatile matter content of PS was significantly higher than that of ZD, whereas the fixed carbon content was opposite, suggesting that PS had a higher pyrolysis reactivity than ZD. The C content of PS was obviously lower than that of ZD, while the contents of O, H and N were opposite. In particular, the O content of PS was about 3.3 times of that of ZD. In Tab. 2 the CaO content of ZD was obviously higher than that of PS, whereas the K_2O, Na_2O, MgO and Al_2O_3 contents were opposite. It indicated that ZD was a high calcium coal in this work.

2.2. Thermogravimetric analysis

The pyrolysis behaviors of PS, ZD and their blends in a linearly heated environment were studied using a thermogravimetry analyzer (TGA, NETZSCH STA 449 F5) which was coupled with a differential scanning calorimetry (DSC) to measure the heat flow into or out of the samples over time. The weight loss change and exothermic phenomenon of each sample were recorded. For each experiment, the sample of about 10 mg was placed in a small crucible, and then put in TGA to study its thermal degradation. The sample was heated from room temperature to 1000 ^{o}C at a heating rate of 20 ^{o}C/min. Nitrogen was used as a carrier gas at a flow rate of 100 ml/min. Each experiment was repeated at least twice to ensure

reproducibility. The thermogravimetric (TG), differential thermogravimetric (DTG) and DSC curves of each sample were obtained using TGA software.

2.3. Analysis of pyrolysis characteristics

The pyrolysis performance is evaluated through the comprehensive pyrolysis index (CPI, $\%^3/(\min^2 \cdot {}^oC^3)$), which is calculated by Eq. (1) [12]:

$$CPI = \frac{(R_p \times R_m) \times m_\infty}{T_i \times T_p \times \Delta T_{1/2}} \quad (1)$$

where R_p is the maximum weight loss rate, %/min; R_m is the average weight loss rate, %/min; m_∞ is the total weight loss, %; T_i is the initial devolatilization temperature, ^oC; T_p is the peak temperature, ^oC; $\Delta T_{1/2}$ is the temperature interval when R/R_p is 1/2, ^oC, and R is the weight loss rate at a certain time, %/min.

To determine the synergistic effect of PS co-pyrolysis with ZD, the experimental values were compared with the calculated ones. The calculated values were obtained by the additive model which supposed that no interactions occurred between two samples during co-pyrolysis [13]. The calculation weight fractions of the blended samples were calculated by Eq. (2).

$$\omega_C = \omega_{PS} \times x + \omega_{ZD} \times (1 - x) \quad (2)$$

where ω_{PS} and ω_{ZD} are the experimental values of the PS and ZD mono-pyrolysis process at the temperature T, respectively; x is the PS blending percentage of the blended sample, %; ω_C is the calculation value of the blended sample.

3. Results and discussion

3.1. Mono-pyrolysis analysis of PS and ZD

The TG and DTG curves of PS and ZD mono-pyrolysis are shown in Fig. 1 (a) and (b), respectively. Generally, the decomposition temperature ranges of the three major components (hemicellulose, cellulose and lignin) of biomass are 200-320 ^oC, 280-400 ^oC, and 140-900 ^oC, respectively [14, 15]. These temperatures were used to predict and analyze the thermal behavior of PS sample in this work. Compared with ZD, PS had much higher content of volatile matter and lower content of fixed carbon in Tab. 1. The mono-pyrolysis process of PS was divided into the three stages with distinct thermal behaviors: drying, release and decomposition of volatile matter, and carbonization. Firstly, at the drying stage, PS was heated, eliminating external moisture with the appearance of drying peak at less than 210 ^oC in Fig. 1 (b). Some light gases were also released at this stage. Secondly, at the release and decomposition stage of volatile matter, ranging from 210 to 540 ^oC, the major weight loss of PS began at 210 ^oC and was closely followed with a drastic increase until a shoulder peak at about 315 ^oC, which was mainly caused by decomposition of hemicellulose [16]. The de-polymerization and decomposition of hemi-cellulose as well as some unstable components of cellulose and lignin produced primary volatile matter [17]. Subsequently, the major weight loss occurred at the second pyrolysis stage and the weight loss peak was determined at 356.6

°C. Meanwhile, lignin underwent further decomposition reaction, and the poly-condensation and aggregation reactions of the newly formed char took place. For the DTG curve of PS pyrolysis in Fig. 1 (b), the slight shoulder at 315 °C corresponds to the degradation of the cellulose in PS, while the main DTG peak at 356.6 °C was consistent with cellulose decomposition [15, 16]. Additionally, the decomposition process of lignin in PS was finished over a wide temperature range of 240-900 °C [18, 19], which caused some tailing peaks in the DTG curves. Finally, at the carbonization stage, which mainly occurred at more than 540 °C, the volatiles generated from PS could form carbonaceous deposits during the pyrolysis process [20]. Meanwhile, the fast pyrolysis reactions of cellulose were finished along with further cracking of lignin and poly-condensation and aggregation reactions of newly formed char [21]. Generally, the TG and DTG curves of PS presented the three main reaction stages following dehydration, devolatilization and char degradation.

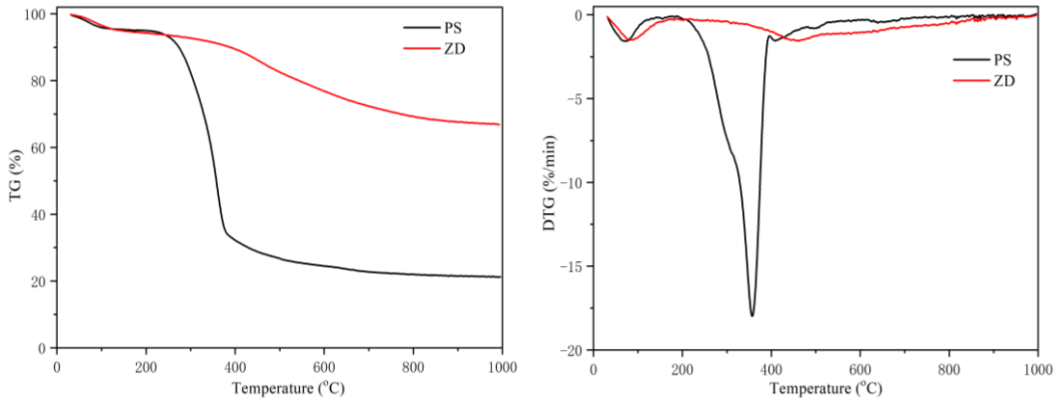

(a) TG (b) DTG

Fig. 1. TG and DTG curves of PS and ZD mono-pyrolysis

As illustrated in Fig. 1, the pyrolysis process of ZD included the following four stages: drying, release and breakdown of light volatile compounds, release and decomposition of heavy compounds, and carbonization. At the first stage of 40-200 °C, the main weight loss processes of ZD included drying, dehydration and removal of gases such as CO_2 and H_2O adsorbed on the surface of ZD particles [22], and the weight loss peak appeared at about 83 °C. At the second stage of 200-300 °C, the release and breakdown of light volatile compounds occurred, which was corresponding to slow pyrolysis process of ZD. Some relatively weak chemical bonds were broken, and functional groups were decomposed to release small molecular gases [22]. The light gases absorbed in the pores of ZD particles began to release along with breaking of unstable functional groups. ZD possessed much lower weight loss of major pyrolysis process over PS, indicating that this stage would release less volatile matter. At the third stage of 300-530 °C, the release and decomposition of heavy volatile compounds occurred. The heavy hydrocarbons were decomposed into the smaller molecular ones, at the same time the light gas species (CO and H_2) were produced [23]. A weight loss peak on the DTG curve of ZD in Fig. 1 (b) was found at 462.0 °C. At the fourth stage of 530-1000 °C, the carbonization process took place. The secondary cracking and polycondensation reactions occurred on the surface of semi-coke or in the semi-coke, causing the conversion of semi-coke to coke. The thermal cracking of ZD at this stage were mainly caused by depolymerization reactions as well as condensation and repolymerization, while the gases,

water vapor, tar and char were formed. Afterwards in the final poly-condensation process, the secondary cracking of tar generated in pyrolysis process occurred followed with further decomposition and shrinkage of ZD char until the end temperature was reached [24].

3.2. Co-pyrolysis analysis

The experimental and calculated curves of all the samples are shown in Fig. 2. The identified corresponding pyrolysis characteristic values were presented in Tab. 3.

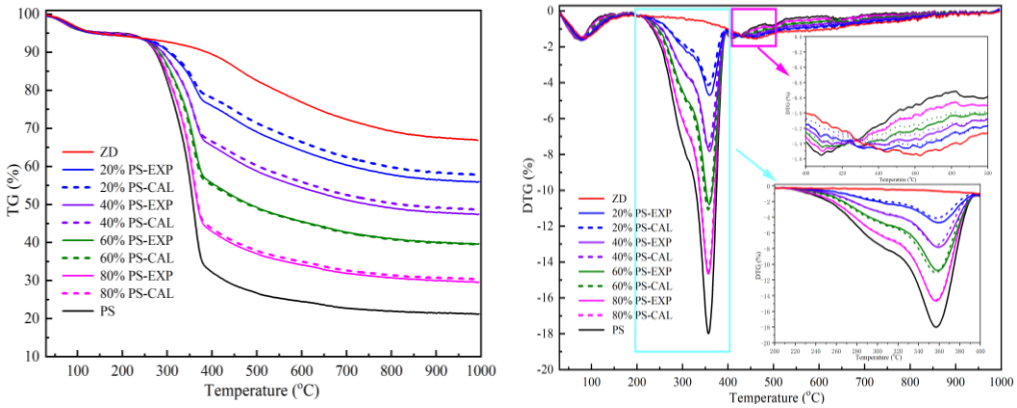

(a) TG (b) DTG

Fig. 2. TG and DTG curves of PS co-pyrolysis with ZD (EXP - Experimental; CAL - Calculated)

From Fig. 2 (a) and (b), the co-pyrolysis curves of PS and ZD existed between the two pure material curves because they possessed the properties of the two materials. Except for the peak of water evaporation at about 100 °C, the pyrolysis process of the PS and ZD blends in the different PS addition percentages showed the three pyrolysis decomposition peaks with the first peak (slight shoulder) at about 320 °C, the second peak at nearly 360 °C, whereas the third peak at approximately 460 °C. Comparing with mono-pyrolysis process, the first two peaks in the PS and ZD blends mainly corresponded to PS decomposition, while the third peak was the result of the presence of ZD in the blends. The second peak, which is R_p, in the co-pyrolysis process in Fig. 2 (b) raised as the adding percentage of PS in the blends increased.

During the co-pyrolysis process of PS and ZD, the presence of PS may influence the pyrolysis reaction process of ZD, whereas the existence of ZD may also affect the pyrolysis reaction process of PS. Therefore, the synergistic effects between PS and ZD are affected by the above two aspects. From Fig. 2, the TG and DTG curves of each blended sample showed thermal behaviors containing both pyrolysis features of PS and ZD. The experimental curves were different from the calculated ones. Besides, the experimental curves of the PS and ZD blends fitted well with the calculation ones when temperature was below 200 °C. As shown in Fig. 2 (a) and (b), when the temperature was more than 300 °C, the experimental TG values of co-pyrolysis were bigger than the calculated TG one at 20, 40 and 80% PS adding percentage, showing that there were obvious positive synergistic effects on weight loss and thermal decomposition rate. It was because PS addition in the co-pyrolysis process supplied hydrogen (H) to the subsequent reactions with ZD [13]. However, the experimental values of co-pyrolysis were less than the calculated one at 60% PS in the main temperature range in Fig. 2 (a) and (b), suggesting the existence of inhibiting effects which reduced weight loss and

thermal decomposition rate. Part of the reason was that the pyrolysis processes of PS and ZD were independent during the co-pyrolysis for cracking and decomposition, resulting in lower residue yields than expected ones. Therefore, it indicated that there were different synergistic effects between PS and ZD in the different PS addition percentages. Whether PS addition into ZD had a synergistic promoting or inhibiting effect in the whole co-pyrolysis process was related to the blending ratio. The similar results in the co-pyrolysis process of coal and biomass were also reported by Chen *et al* [25].

Compared with ZD, PS contained more oxygen content and released more volatiles, which contained a more oxygenated species. Additionally, the volatiles from PS pyrolysis could react with ZD particles during the co-pyrolysis process [26]. The decomposition reactions of PS could release gases more rapidly than ZD due to the relatively lower bond energies of ether and C-C bonds associated with lignocellulosic biomass, compared to the C-C aromatic bonds typically found in the molecular structure of ZD [27]. The main pyrolysis stage of the PS and ZD blends was in the temperature range of 200-428 ^{o}C, in which PS underwent main pyrolysis reactions and released a large amount of volatiles. Although ZD began in the initial pyrolysis process at 368.6 ^{o}C, its matrix only underwent preliminary depolymerization and decomposition reactions with releasing a small amount of volatiles. Therefore, the interaction reactions between the volatile matter of ZD and the char of PS near 356.6 ^{o}C were the main mechanism of synergistic effect in the decomposition process of volatile compounds. Moreover, within the temperature range of 428-500 ^{o}C in Fig. 2 (b), the experimental DTG values of the PS and ZD blends were bigger than the calculated DTG one at 20, 40 and 80% PS adding percentage, showing that there were obvious positive synergistic interactions. The main pyrolysis of ZD was near 462.0 ^{o}C, in which it underwent strong pyrolysis reactions and released a large amount of volatiles. Although PS was at the carbonization stage at around 462.0 ^{o}C, its matrix mainly underwent aromatization of saturated hydrocarbons and dehydrocondensation of aromatic rings with releasing a small amount of light gases. So, the interaction reactions between the volatiles of PS and the char of ZD near 462.0 ^{o}C were the main mechanism of synergistic effect in the carbonization process. Compared with ZD, PS contained more alkali and alkaline earth metallic species such as K and Na, which catalyzed the secondary cracking of volatiles and their precursors, thus increasing the devolatilization rate and reducing peak temperatures of co-pyrolysis [28]. Generally, R_p and R_m of co-pyrolysis in Tab. 3 showed an increasing trend with PS addition percentage.

Tab. 3. Pyrolysis characteristic parameters for PS, ZD and their blends

Samples	EXP/CAL	T_i (℃)	$\Delta T_{1/2}$ (℃)	R_p (%/min)	T_p (℃)	R_m (%/min)	m_f (%)	m_∞ (%)	*CPI* (%^{3}/(min^2·℃^{3}))
ZD	EXP	368.6	314.0	-1.55	462.0	-0.70	66.88	33.12	6.72E-07
20% PS	EXP	304.0	64.0	-4.70	359.4	-0.92	55.99	44.01	2.72E-05
	CAL	305.1	63.0	-4.12	356.4	-0.88	57.75	42.25	2.24E-05
40% PS	EXP	309.7	60.0	-7.83	359.1	-1.10	47.48	52.52	6.78E-05
	CAL	309.0	59.0	-7.59	356.1	-1.07	48.62	51.38	6.40E-05
60% PS	EXP	309.0	56.0	-10.79	359.1	-1.26	39.68	60.32	1.32E-04
	CAL	306.9	56.0	-11.06	356.1	-1.26	39.49	60.51	1.38E-04

80% PS	EXP	307.9	56.0	-14.67	357.1	-1.47	29.64	70.36	2.46E-04
	CAL	310.8	55.0	-14.52	356.1	-1.45	30.36	69.64	2.41E-04
PS	EXP	310.8	54.6	-17.99	356.6	-1.64	21.26	78.74	3.84E-04

The residual char yield (m_f) from the experimental curve in Tab. 3 was lower than that from the calculated curve at 20%, 40% or 80% PS, indicating that there were some positive synergistic effects which promoted cracking and decomposition of chemical compounds. Compared with ZD, PS had a higher H/C, making PS act as a H_2-donor in the co-pyrolysis process [13]. This positive effect could be caused by the hydroxide (OH) and H radicals formed from the PS pyrolysis transferring to the ZD structure, improving the decomposition of ZD [29]. The H/C and O/C ratios of PS in Tab. 1 were about 3.0 and 4.7 times higher than those of ZD, respectively. Therefore, many H and OH radicals could be produced and used as H donor species, enhancing the decomposition of ZD and decreasing the co-pyrolysis residual yield [30]. Further, secondary reactions, such as depolymerization and repolymerization reactions, were improved by the H-transferring behavior in the PS and ZD blends, reducing secondary char and tar formation. Song *et al* [31] also discovered that biomass pyrolysis was the first step in the co-pyrolysis process of biomass and coal, and the H_2 produced was applied as an outer hydrogenation reaction source for coal pyrolysis. Additionally, the catalytic effect of AAEMs in PS enhanced the decomposition and releasing of heavy compounds during the PS and ZD co-pyrolysis, enhancing the synergy effect [32]. Based on the data analysis of the co-pyrolysis process in Fig. 2 and Tab. 3, the experimental values of the PS and ZD blends in the different blending ratios were higher and lower than the calculated values, indicating that there were both synergistic promoting and inhibiting effects in the whole co-pyrolysis process of PS and ZD.

3.3. Kinetic analysis

Coats-Redfern was used to investigate the kinetic parameters in terms of the activation energy (E), pre-exponential factor (A) and correlation coefficient (R^2) for mono-pyrolysis and co-pyrolysis based on the first-order reaction model [33]. The average activation energy (E_0) in the whole pyrolysis process was calculated according to the literature [34]. The kinetic parameters of PS, ZD and their blends in the different blending ratios are shown in Tab. 4.

The R^2 values of all the samples in Tab. 4 were more than 0.93, showing that the employed the first-order reaction model could describe the pyrolysis processes very well. The pyrolysis process of PS, ZD and their blends could be described by the two consecutive first-order reactions in two different temperature intervals. Stage ① and ② in Tab. 4 mainly represents the decomposition stage and the carbonization stage, respectively. Generally, the E values required for the thermal decomposition of cellulose, hemicellulose and lignin are 128-263, 90-165 and 20-100 kJ/mol, respectively [35]. E_0 of PS in Tab. 4 was the biggest due to the complex and stable structure nature of PS compared with ZD. For the PS and ZD blends, as the PS adding percentage increased, the E value at Stage ① first decreased then increased, getting the minimum value of 92.00 kJ/mol at 60% PS percentage. However, the E value at Stage ② increased firstly and then decreased with an increase of PS adding percentage, reaching the maximum value of 228 kJ/mol at 40% PS percentage. These

change trends could be attributed to the complex pyrolysis reaction routes, mainly parallel complex reactions [36]. The lowest E that was required to initiate the reaction was determined to be 92.00 kJ/mol at 60% PS percentage at Stage ①. Generally, as the adding percentage of PS into ZD increased, the E_0 value of the blends gradually increased. This result was also obtained by Wang *et al*. [9] who reported that a significant reduce of E has been observed when adding wood to bituminous coal. Additionally, the E_0 value for each blend was lower than that of PS or ZD, implying that the synergistic promoting effect on the co-pyrolysis process was significant. This can be attributed to the fact of PS is mainly made up of hemicellulose, cellulose and lignin whereas ZD is composed of a number of complex components. For the co-pyrolysis of PS and ZD, the above kinetic results may mean that the synergistic effect can reduce the reaction energy input during the co-pyrolysis reaction, which is attractive for engineering applications.

Tab. 4. Results of the kinetic parameters of different samples

Samples	Stages	Temperature ranges (°C)	A (min^{-1})	E ($kJ \cdot mol^{-1}$)	R^2	E_0 ($kJ \cdot mol^{-1}$)
ZD	①	300-530	6.06×10^{8}	49.00	0.94779	128.94
	②	530-610	2.09×10^{13}	211.00	0.95553	
20% PS	①	225-385	8.49×10^{7}	135.00	0.99493	105.89
	②	385-521	2.65×10^{14}	209.00	0.96072	
40% PS	①	229-383	8.65×10^{9}	134.00	0.99711	106.91
	②	383-527	3.54×10^{13}	228.00	0.96507	
60% PS	①	232-364	1.98×10^{10}	92.00	0.99316	115.84
	②	364-443	3.22×10^{13}	203.00	0.93359	
80% PS	①	210-377	8.34×10^{8}	103.00	0.98749	118.38
	②	377-510	6.22×10^{12}	178.00	0.98257	
PS	①	210-540	1.89×10^{12}	199.00	0.9815	191.55
	②	540-610	4.55×10^{13}	225.00	0.98250	

3.4. SEM analysis

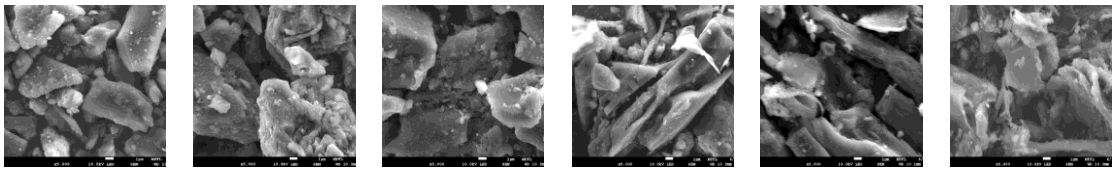

(a) ZD (b) 20% PS (c) 40% PS (d) 60% PS (e) 80% PS (f) PS

Fig. 3. SEM images of char residues from different samples (5000 × magnification)

The SEM images (5000 × magnification) of the char residues obtained after TGA experiments are shown in Fig. 3. These images could present the change of char surface morphology, showing the results from the synergistic effects of PS co-pyrolysis with ZD. From the images of mono-pyrolysis chars of ZD and PS in Fig. 3 (a) and (f), the particles of ZD were different from those of PS. The surface of PS char particles presented an irregular stick-shaped morphology with abundant cavities and porous structures due to the violent release of volatile matter in PS. PS char framework with columnar morphology had some irregular crystal particles at the surface, which might be condensed ashes with low melting point that released during pyrolysis [37]. They were caused by softening and melting during

deep poly-condensation of PS in high temperature intervals [38]. However, the ZD char surface appeared to be smooth and showed a granular and blocky structure. This was attributed to high carbonation degree in the ZD pyrolysis process. ZD char represented rough morphology with plenty protuberances, and had relatively smoother surface consisting of dense hydrocarbon molecules. In the chars derived from the co-pyrolysis of the PS and ZD blends in Fig. 3 (b)-(e), the morphology of the co-pyrolysis chars clearly changed from that seen with ZD char into a granular and loose packed structure with an increase of PS addition. These changes were likely relevant to the increased reactivity of the chars derived from the PS and ZD blends. For the co-pyrolysis chars, the traces of coke and deposit could be found in Fig. 3 (b)-(e), presenting dense discrete crystal coverings on the surface. These were caused by gas-solid interactions. The marked differences of thermal decomposition and void spaces between PS and ZD created some favorable conditions for volatile adsorption and carbonization, which should be the primary cause of synergy observed in TGA curves. Meanwhile, the volatile matter released by PS pyrolysis could greatly affect the porous structures of co-pyrolysis chars.

4. Conclusions

The co-pyrolysis characteristics, kinetic parameters and char surface morphology of poplar sawdust (PS) with Zhundong coal (ZD) were investigated via thermogravimetric analysis in this work. The synergistic effects of co-pyrolysis in the different aspects were also explored. The results showed that the mono-pyrolysis process of PS was divided into the three stages including drying, release and decomposition of volatile matter, and carbonization. The pyrolysis process of ZD included the following four stages: drying, release and breakdown of light volatile compounds, release and decomposition of heavy compounds, and carbonization. Whether PS addition into ZD had a synergistic promoting or inhibiting effect in the whole co-pyrolysis process was related to the PS addition percentage. There were some positive synergistic effects which promoted the cracking and decomposition rate at 20%, 40% and 80% PS addition, while at 60% PS there existed an inhibiting effect which would reduce pyrolysis reaction rate. As the adding percentage of PS into ZD increased, the average activation energy of the blends gradually increased. The morphology of the co-pyrolysis chars gradually turned a granular and loose packed structure with an increase of PS addition. The kinetic parameters of PS and ZD pyrolysis process were obtained by the activation energy model method. The obtained results are important for high-efficiency design and operation of co-pyrolysis system of PS and ZD.

Acknowledgements

This research has received the support of the Basic Research Program of Natural Sciences of Shaanxi Province (No. 2023-JC-YB-406).

References

[1] Tokimatsu, K., *et al*., Global zero emissions scenarios: The role of biomass energy with carbon capture and storage by forested land use, *Applied Energy*, 185 (2017), pp. 1899-1906.

[2] Li, S., *et al*., Study on co-pyrolysis characteristics of rice straw and Shenfu bituminous coal blends in a fixed bed reactor, *Bioresource Technology*, 155 (2014), pp. 252-257.

[3] Lu, Y., *et al.*, The characteristics of mineralogy, morphology and sintering during co-combustion of Zhundong coal and oil shale, *RSC advances*, 7 (2017), 81, pp. 51036-51045.

[4] Zhang, Z., *et al.*, Recent advances in carbon dioxide utilization, *Renewable and Sustainable Energy Reviews*, 125 (2020), 109799.

[5] Castells, B., *et al*., Kinetic study of different biomass pyrolysis and oxygen-enriched combustion, *Thermal Science*, 26 (2022), 5B, pp. 4131-4145.

[6] Gouws, S. M., *et al*., Co-pyrolysis of coal and raw/torrefied biomass: A review on chemistry, kinetics and implementation, *Renewable and Sustainable Energy Reviews*, 135 (2021), 110189.

[7] Gohar, H., *et al*., Investigating the characterisation, kinetic mechanism, and thermodynamic behaviour of coal-biomass blends in co-pyrolysis process, *Process Safety and Environmental Protection*, 163 (2022), pp. 645-658.

[8] Shafizadeh, A., *et al*., Machine learning-enabled analysis of product distribution and composition in biomass-coal co-pyrolysis, *Fuel.* 355 (2024). 129464.

[9] Wang, W., *et al*., Thermogravimetric analysis and kinetic modeling of the co-pyrolysis of a bituminous coal and poplar wood, *Chinese Journal of Chemical Engineering*, 58 (2023), pp. 53-68.

[10] Wu, Z., *et al*., Co-pyrolysis of lignocellulosic biomass with low-quality coal: Optimal design and synergistic effect from gaseous products distribution, *Fuel*, 236 (2019), pp. 43-54

[11] Ruan, R., *et al*., Evolution of particulate matter in the post-combustion zone of Zhundong lignite, *Fuel*, 281 (2020), 118780.

[12] Zhang, J., *et al*., TG-FTIR and Py-GC/MS analyses of pyrolysis behaviors and products of cattle manure in CO_2 and N_2 atmospheres: Kinetic, thermodynamic, and machine-learning models, *Energy conversion and management*, 195 (2019), pp. 346-359.

[13] Park, D., *et al*., Co-pyrolysis characteristics of sawdust and coal blend in TGA and a fixed bed reactor, *Bioresource Technology*, 101 (2010), 15, pp. 6151-6156.

[14] Stefanidis, S. D., *et al*., A study of lignocellulosic biomass pyrolysis via the pyrolysis of cellulose, hemicellulose and lignin, *Journal of analytical and applied pyrolysis*, 105 (2014), pp. 143-150.

[15] Yang, H., *et al*., Characteristics of hemicellulose, cellulose and lignin pyrolysis, *Fuel*, 86 (2007), 12-13, pp. 1781-1788.

[16] Chen, D., *et al*., Insight into biomass pyrolysis mechanism based on cellulose, hemicellulose, and lignin: Evolution of volatiles and kinetics, elucidation of reaction

pathways, and characterization of gas, biochar and bio-oil, *Combustion and Flame*, 242 (2022), 112142.

[17] Di Nola, G., *et al*., TG-FTIR characterization of coal and biomass single fuels and blends under slow heating rate conditions: Partitioning of the fuel-bound nitrogen, *Fuel Processing Technology*, 91 (2010), 1, pp. 103-115.

[18] Wu, Z., *et al*., Synergistic effect on thermal behavior during co-pyrolysis of lignocellulosic biomass model components blend with bituminous coal, *Bioresource Technology*, 169 (2014), pp. 220-228.

[19] Lv, G., *et al*., Analytical pyrolysis studies of corn stalk and its three main components by TG-MS and Py-GC/MS, *Journal of Analytical and Applied Pyrolysis*, 97 (2012), pp. 11-18.

[20] Darmstadt, H., *et al*., Co-pyrolysis under vacuum of sugar cane bagasse and petroleum residue properties of the char and activated char products, *Carbon*, 39 (2001),6, pp. 815-825.

[21] Lin, B., *et al.*, Thermal behavior and gas evolution characteristics during co-pyrolysis of lignocellulosic biomass and coal: A TG-FTIR investigation, *Journal of Analytical and Applied Pyrolysis*, 144 (2019), 104718.

[22] Shi, L., *et al*., Pyrolysis behavior and bonding information of coal - A TGA study, *Fuel Processing Technology*, 108 (2013), pp. 125-132.

[23] Seo, D. K., *et al*., Study of coal pyrolysis by thermo-gravimetric analysis (TGA) and concentration measurements of the evolved species, *Journal of Analytical and Applied Pyrolysis*. 92, (2011), 1, pp. 209-216.

[24] Song, H., *et al*., Pyrolysis characteristics and kinetics of low rank coals by TG-FTIR method, *Fuel Processing Technology*, 156 (2017), pp. 454-460.

[25] Chen, X., *et al*., Pyrolysis characteristics and kinetics of coal–biomass blends during co-pyrolysis, *Energy & Fuels*, 33 (2019), 2, pp. 1267-1278.

[26] Sonobe, T., *et al*., Synergies in co-pyrolysis of Thai lignite and corncob, *Fuel Processing Technology*, 89 (2008), 12, pp. 1371-1378.

[27] Moghtaderi, B., *et al*., Pyrolytic characteristics of blended coal and woody biomass, *Fuel*, 83 (2004), 6, pp. 745-750.

[28] Zhang, Y., *et al*., Capture of released alkali metals and its simultaneously catalytic performance on secondary reactions of volatiles during biomass pyrolysis, *Fuel*, 317 (2022), 123557.

[29] Soncini, R. M., *et al*., Co-pyrolysis of low rank coals and biomass: Product distributions, *Fuel*, 112 (2013), pp. 74-82.

[30] Yuan, S., *et al*., Rapid co-pyrolysis of rice straw and a bituminous coal in a high-frequency furnace and gasification of the residual char, *Bioresource Technology*, 109 (2012), pp. 188-197.

[31] Song, Y., *et al.* Pathway of biomass-potassium migration in co-gasification of coal and biomass, *Fuel*, 239 (2019), pp. 365-372.

[32] Hosokai, S., *et al.*, Spontaneous generation of tar decomposition promoter in a biomass steam reformer, *Chemical engineering research and design*, 83 (2005), 9, pp. 1093-1102.

[33] Apaydin-Varol, E., *et al*., Pyrolysis kinetics and thermal decomposition behavior of polycarbonate-a TGA-FTIR study, *Thermal Science*, 18 (2014), 3, pp. 833-842.
[34] Li, J., *et al*., Biochar-Assisted Catalytic Pyrolysis of Oily Sludge to Attain Harmless Disposal and Residue Utilization for Soil Reclamation, *Environmental Science & Technology*, 57 (2023), 13, pp. 7063-7073.
[35] Li, Z., *et al*., Kinetic study of corn straw pyrolysis: comparison of two different three-pseudocomponent models, *Bioresource Technology*, 99 (2008), 16, pp. 7616-7622.
[36] Ma, Z., *et al*., Determination of pyrolysis characteristics and kinetics of palm kernel shell using TGA-FTIR and model-free integral methods, *Energy Conversion and Management*, 89 (2015), pp. 251-259.
[37] Guo, F., *et al*., Characterization of Zhundong lignite and biomass co-pyrolysis in a thermogravimetric analyzer and a fixed bed reactor, *Energy*, 141 (2017), pp, 2154-2163.
[38] Fu, P., *et al*., Evolution of char structural features during fast pyrolysis of corn straw with solid heat carriers in a novel V-shaped down tube reactor, *Energy Conversion and Management*, 149 (2017), pp. 570-578.

Paper submitted: 24.03.2024
Paper revised: 08.08.2024
Paper accepted: 15.08.2024